catalysts

MDPI

Article

Morphology Regulation Mechanism and Enhancement of Photocatalytic Performance of BiOX (X = Cl, Br, I) via Mannitol-Assisted Synthesis

Patrycja Wilczewska [1], Aleksandra Bielicka-Giełdoń [1,*], Karol Szczodrowski [2], Anna Malankowska [1], Jacek Ryl [3], Karol Tabaka [1] and Ewa Maria Siedlecka [1]

[1] Faculty of Chemistry, University of Gdansk, Wita Stwosza 63, 80-308 Gdansk, Poland; patrycja.wilczewska@phdstud.ug.edu.pl (P.W.); anna.malankowska@ug.edu.pl (A.M.); karol.tabaka@phdstud.ug.edu.pl (K.T.); ewa.siedlecka@ug.edu.pl (E.M.S.)
[2] Faculty of Mathematics, Physics and Informatics, University of Gdansk, Wita Stwosza 57, 80-308 Gdansk, Poland; karol.szczodrowski@ug.edu.pl
[3] Institute of Nanotechnology and Materials Engineering, Faculty of Applied Physics and Mathematics, Gdansk University of Technology, Narutowicza 11/12, 80-233 Gdansk, Poland; jacek.ryl@pg.edu.pl
* Correspondence: a.bielicka-gieldon@ug.edu.pl; Tel.: +48-585235226

Abstract: BiOX (X = Cl, Br, I) photocatalysts with dominant (110) facets were synthesized via a mannitol-assisted solvothermal method. This is the first report on the exposed (110) facets-, size-, and defects-controlled synthesis of BiOX achieved by solvothermal synthesis with mannitol. This polyol alcohol acted simultaneously as a solvent, capping agent, and/or soft template. The mannitol concentration on the new photocatalysts morphology and surface properties was investigated in detail. At the lowest concentration tested, mannitol acted as a structure-directing agent, causing unification of nanoparticles, while at higher concentrations, it functioned as a solvent and soft template. The effect of exposed (110) facet and surface defects ($Bi^{(3-x)+}$, Bi^{4+}, Bi^{5+}) of BiOX on the photocatalytic activity of nanomaterials under the UV–Vis irradiation were evaluated by oxidation of Rhodamine B (RhB) and 5-fluorouracil (5-FU), an anticancer drug, and by reduction of Cr(VI). Additionally, the influence of crucial factors on the formation of BiOX in the synthesis with mannitol was discussed extensively, and the mechanism of BiOX formation was proposed. These studies presented a new simple method for synthesizing BiOX without any additional surfactants or shape control agents with good photocatalytic activity. The study also provided a better understanding of the effects of solvothermal conditions on the BiOX crystal growth.

Keywords: BiOX; photocatalysis; mannitol; soft template; structure-directing agent

Citation: Wilczewska, P.; Bielicka-Giełdoń, A.; Szczodrowski, K.; Malankowska, A.; Ryl, J.; Tabaka, K.; Siedlecka, E.M. Morphology Regulation Mechanism and Enhancement of Photocatalytic Performance of BiOX (X = Cl, Br, I) via Mannitol-Assisted Synthesis. *Catalysts* **2021**, *11*, 312. https://doi.org/10.3390/catal11030312

Academic Editors: Sophie Hermans and Julien Mahy

Received: 29 January 2021
Accepted: 23 February 2021
Published: 26 February 2021

1. Introduction

Bismuth oxyhalides BiOX (X = Cl, Br, I) are among the most important groups of semiconductors and have drawn considerable attention for their potential applications as novel photocatalysts active in ultraviolet, visible, and UV–Vis light [1]. BiOX crystalizes in the tetragonal structure of the matlockite with slabs $[Bi_2O_2]^{2+}$ interleaved by slabs of halogen $[X]^-$. These layered structures affect highly anisotropic electrical, magnetic, and optical properties and make BiOX promising materials in wide industrial and environmental applications [1,2].

Inorganic materials' physical and chemical features, especially optical, magnetic, and electronic properties depending on size, dimensions, and morphology, are also strongly related to the morphology and dimensionality of the semiconductors in their photocatalytic activity [1]. Over the years, many efforts have been made to synthesized BiOX with different morphology such as nanobelts [3], nanowires [4], nanosheets [5], nanoplates [6], nanotubes [3], nanoparticles [7], nanoflowers [8], lamella structures [9], hollow structures [10], and hierarchical nanostructures [6,7].

Additionally, within described types of structure, attempts of facet engineering were made [8,11].

One of the common methods of obtaining various nanomaterials and BiOX itself is solvothermal synthesis. Fabrication of bismuth oxychloride (BiOCl) using ethanol (ETH) [12], ethylene glycol (EG) [13–15], diethylene glycol (DEG) [14,15], triethylene glycol (TEG) [14], glycerol (GLY) [16,17], *N*,*N*-dimethylformamide (DMF) [7,14], polyethylene glycol (PEG) [13,18], water [14,18,19], and mannitol (MAN) [15,19] in the temperature range from 140 °C to 160 °C and the time of 3–16 h was studied. Bismuth oxybromide has so far been obtained from water [20,21], ethanol [22–24], isobutanol (ISO) [21], ethylene glycol [20–22,24,25], glycerol [21,22,24], and mannitol [25] under condition of 20–160 °C and 8–15 h. Solvothermal synthesis of bismuth oxyiodine used EG [26,27], ETH [26,27], GLY [26], and water [26] as solvents, and the autoclave reactions were conducted in 160 °C for 12 h.

Additionally, a few studies have focused on interactions between bismuth and halogens precursor, surfactants, and the solvent mixtures' effect on these nanomaterials' morphology. BiOXs have been prepared by the solvothermal method with many surfactants—tetrabutylammonium halides [12], hexadecyltrimethylammonium halides [28], cetylpyridinium halide [25], polyvinyl pyrrolidone [29], polyvinyl alcohol [30], and sodium dodecyl sulfate [31]). Surfactants were used as templates during the synthesis reaction process. The physical and chemical properties of BiOCl were tunable by mixing PEG and water [18] or TEG and DMF [7] in different volume ratios. A similar investigation for BiOI with EG and water mixture was also conducted [26].

Although many different methods have been developed to modulate the morphology and crystallites size of BiOX (X = Cl, Br, I), expensive surfactants and various organic solvents were usually used for synthesis. Because the solvent plays a significant role in controlling bismuth oxyhalides' morphology, it is crucial to develop an additive-free synthesis method, which will be more convenient to fabricate these semiconductors. Moreover, the development of alternative ecological synthesis for nanomaterials may reduce the negative impact of widely used chemicals on human health and the environment. A control of semiconductor morphology is a promising approach to improve the photocatalytic activity of BiOX and should be investigated more thoroughly.

Mannitol (MAN) is a type of sugar alcohol used as a sweetener. Due to its excellent mechanical compressing properties and physical-chemical stability, it is used to produce pharmaceuticals. Furthermore, toxicity studies indicated that mannitol did not cause any considerable adverse effects. As an environmentally friendly and cheap bio-polyol, MAN can be used to prepare nanomaterial due to the presence of a long carbon chain and multi-hydroxyl groups. It was reported that the presence of mannitol during the synthesis favored the formation of uniform nanostructures [25], which is desirable in photocatalytic processes. However, information on mannitol as a solvent in the semiconductors' synthesis and their photoactivity is limited and requires further research.

This study described the effects of mannitol concentration (0.1 M, 0.5 M, and 1 M) on the (110) planes exposition and defects in the crystal lattice of BiOX material (where X = Cl, Br, I), enhancing its photoactivity in oxidation and reduction of micropollutants. Moreover, such prepared photocatalysts were used for the first time to cytostatic drug (5-fluorouracil (5-FU)) removal from water.

To the best of our knowledge, this is the first report on the exposed (110) facets-, size- and defects-controlled synthesis of BiOX (X = Cl, Br, I) achieved by solvothermal synthesis with mannitol as a solvent, capping agent, and/or soft template simultaneously. This research provides a new, simple strategy to fabricate BiOX without any additional surfactants or shape-controlled agents and enhanced photocatalytic activity. The obtained results indicated that BiOX prepared in mannitol solution could be used to remove a wide range of water micropollutants, including cytostatic drugs such as 5-fluorouracil.

2. Results and Discussion

2.1. Characterization

2.1.1. XRD Analysis

The purity and crystallinity of prepared BiOX photocatalysts were examined by X-ray powder diffraction (XRD). Figure 1 shows the XRD patterns of synthesized BiOX by the mannitol-assisted solvothermal method.

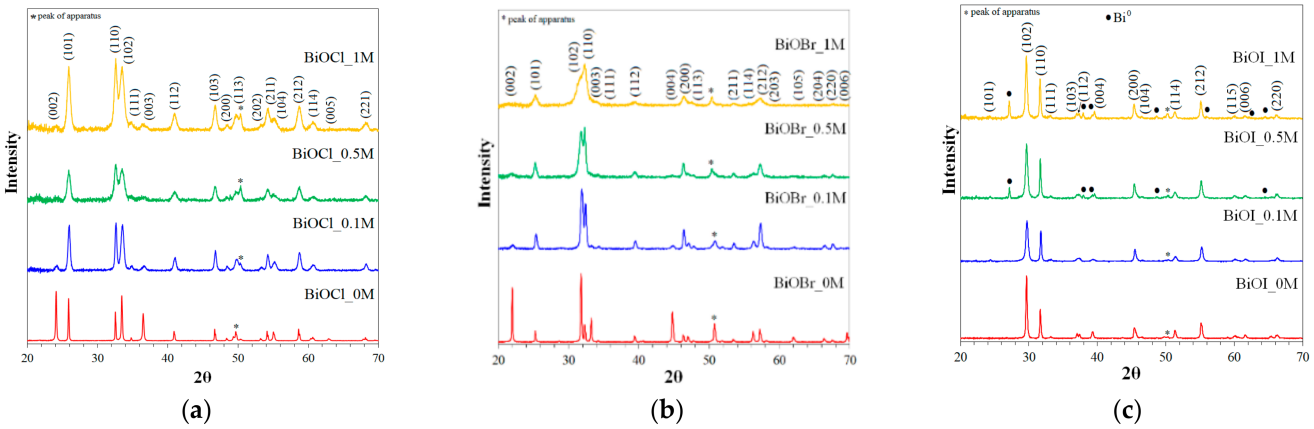

Figure 1. X-ray powder diffraction (XRD patterns) of (**a**) BiOCl, (**b**) BiOBr, and (**c**) BiOI prepared in synthesis with different mannitol concentrations.

As shown in Figure 1a, all diffraction peaks of BiOCl could be indexed to the tetragonal phase BiOCl (PDF 04-002-3608). No other diffraction peaks were detected, indicating the high purity of BiOCl. The signals of BiOCl_0M and BiOCl_0.1M diffractograms were intense, sharp, and narrow suggesting the high crystallinity of the samples. The higher concentration of the mannitol solution resulted in the formation of smaller crystallites, which can be observed as wider and shorted peaks in the BiOCl_0.5M and BiOCl_1.0M diffractograms [14,32]. The crystallite sizes obtained from the Scherrer equation and the half-maximum full width of the signal decreased from 95 nm (BiOCl_0M) to 32 nm (BiOCl_1M). In the absence of mannitol in the synthesis process, diffraction peaks of BiOCl_0M photocatalyst at 24.2°, 36.6°, 49.6°, and 63.2° have corresponded {001} family of planes. In contrast to distilled water, mannitol inhibited the formation of {001} planes due to the interaction of the hydroxyl groups of mannitol molecules and oxygen atoms in BiOCl (001) facets through hydrogen bonds. This phenomenon limited the growth along the [001] orientation of the BiOCl crystals, and the peaks of these family planes had lower intensity than the sample prepared in ultrapure water.

The XRD patterns of BiOBr are presented in Figure 1b. Signals were well-fitted to BiOBr (PDF 04-002-3609). The signals of BiOBr_0M were the sharpest and narrowest, similarly to the BiOCl series than the other BiOBr. The crystallite size of BiOBr was 90 nm and decreased after the introduction of the mannitol to the synthesis to 42 nm (BiOBr_0.1M). The rest of the BiOBr samples could not determine the crystallites' size from the most intense signal due to its poor separation. Bismuth oxybromide synthesized in ultrapure water (BiOBr_0M) was characterized by the {001} family of planes in the structure. In contrast, these planes' signals were absent in the series of BiOBr samples prepared in mannitol solutions. Furthermore, as previously described, the hydroxyl groups of alcohols are preferentially adsorbed on the (102) facets by the coordination of exposed Bi^{3+} ions, thus inhibiting growth along the (102) direction [33].

Our study observed these phenomena in preparation of a series of BiOBr (BiOBr_0.1M, BiOBr_0.5M, and BiOBr_1M), while this trend was not found for BiOCl. This fact could be related to the weak force interaction between mannitol and the smaller BiOCl particles. The diffraction intensity ratio (I_{110}/I_{102}) of the BiOX photocatalysts, listed in Table 1, increased with the increase of the mannitol concentration. The (110) and (102) facets were preferred

for generation and accumulation of free e^- for the reduction reaction than other crystal facets [34,35]. Knowledge of the BiOX facets responsible for reduction is still limited in contrast to the oxidation processes connected with facets (001) and (010) [11,20].

Table 1. Physicochemical properties of BiOX (X = Cl, Br, I) samples synthesized in ultrapure water and mannitol solutions.

Photocatalyst	Particle Size	Morphology	Eg (eV)	MVB (eV)	MCB (eV)	I_{110}/I_{102}
BiOCl_0M	0.48–1.9 µm	microplate	3.3	3.51	0.21	0.65
BiOCl_0.1M	41.3–66.6 nm	nanoplate	3.2	3.46	0.26	1.03
BiOCl_0.5M	13.4–25.4 nm	nanoplate	3.05	3.38	0.33	1.14
BiOCl_1M	15–20 nm	nanoparticle	3.0	3.36	0.36	1.13
BiOBr_0M	1.45–5.12 µm	microplate	2.58	2.99	0.41	0.25
BiOBr_0.1M	40.8–81.0 nm	nanoplate	2.65	3.03	0.38	0.76
BiOBr_0.5M	58.5–72.7 nm	nanoplate	2.65	3.03	0.38	1.08
BiOBr_1M	530–734 nm	microstructure flower-like	2.56	2.98	0.42	1.40
BiOI_0M	4.13–5.65 µm	microplate	1.65	2.26	0.61	0.46
BiOI_0.1M	0.74–1.21 µm	microstructure rose-like	1.65	2.26	0.61	0.75
BiOI_0.5M	0.74–1.21 µm	microplate	1.58	2.23	0.65	0.72
BiOI_1M	183–361 nm	nanoplate	1.50	2.19	0.69	0.63

Figure 1c shows the XRD patterns of the BiOI samples prepared in highly purified water as a reference sample and mannitol solution. All samples could be indexed as BiOI (PDF 04-012-5693). The XRD results indicated that the series of BiOI photocatalysts synthesized by the solvothermal method were well crystallized and of high purity. The crystallite sizes of BiOI_0M, BiOI_0.1M, BiOI_0.5M, and BiOI_1M were 73.6 nm, 41.0 nm, 45.7 nm, and 52.6 nm, respectively. BiOI photocatalysts prepared in pure water and 0.1 M solution of mannitol (BiOI_0.1M) were characterized by almost identical XRD patterns. As previously described for the series of BiOCl and BiOBr, the samples prepared in a higher concentration of mannitol than 0.1 M the {001} planes were not formed. This phenomenon could be explained by the larger ionic radius of I^- than Br^- and Cl^- ionic radius and their various spatial packing of ions on the plane.

Furthermore, in the series of BiOI, the type of solvent used for the sample synthesis influenced the appearance of the additional Bi^0 phase. Increasing the concentration of mannitol from 0.1 M to 0.5 M and 1 M led to the formation of 12% and 17% of the Bi^0 phase in BiOI materials, respectively. It can be explained by the reducing properties of mannitol and its redox reaction with Bi^{3+} ions. It was previously reported that the organic compounds used in the synthesis, such as Na_2EDTA [36] and ethylene glycol [37], were capable of reducing metal ions at a high temperature of solvothermal synthesis. The appearance of Bi^0 in BiOI samples was probably related to a slower formation of bismuth oxyiodine nanosheets than other oxyhalides nanosheets and longer time of free Bi^{3+} ions exposition to the interaction with reductive mannitol. The slower formation of BiOI nanoplates due to the large radius of iodide ions was the reason for the favorable reduction of bismuth ions. Slower formation of BiOI was also observed after the introduction of Na_2EDTA, which could complex Bi^{3+} to the synthesis, and the rate of obtaining bismuth oxyiodide was decreased with increasing concentration of Na_2EDTA [38]. The obtained results revealed relevant coordination interactions between solvents and precursors in the formation of BiOX and were specific to each type of halide. Moreover, high crystallinity and purity, which are considered essential factors influencing nanomaterials' photocatalytic properties, were also solvent-dependent.

2.1.2. SEM Analysis

The morphologies and structures of selected BiOX (X = Cl, Br, I) photocatalysts examined by scanning electron microscopy are shown in Figure 2. The size and morphology of the samples are listed in Table 1.

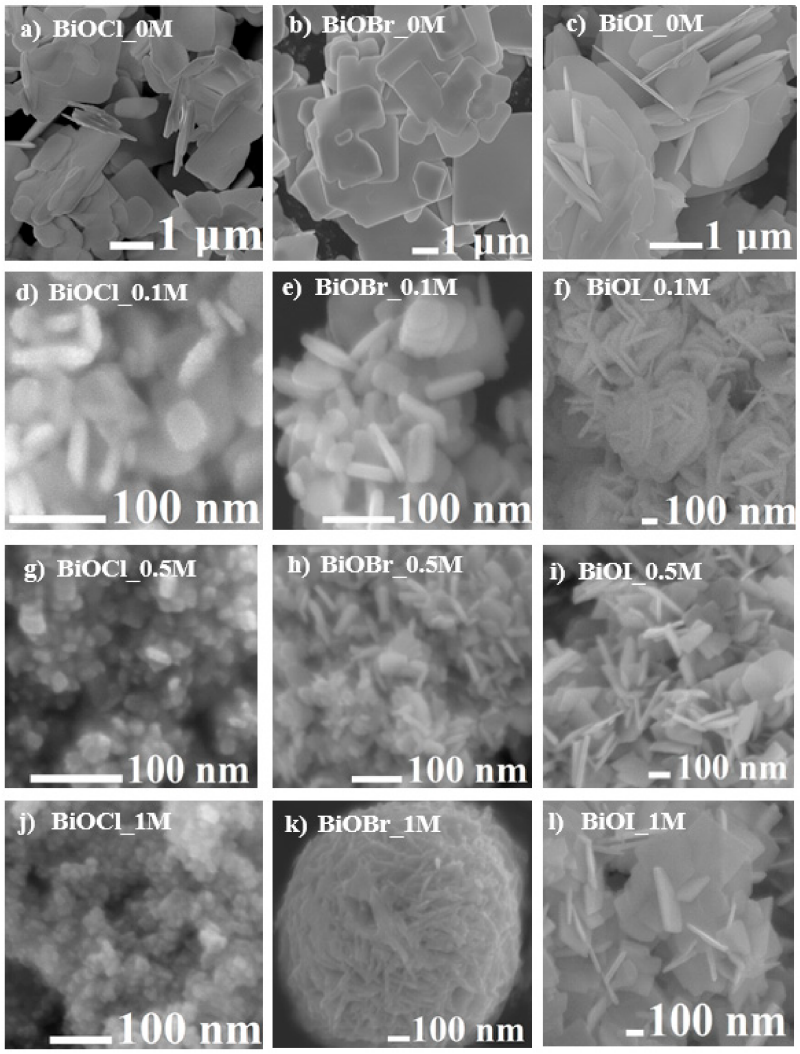

Figure 2. SEM images of BiOX synthesized in (**a**–**c**) water; (**d**–**f**) 0.1 M mannitol solution; (**g**–**i**) 0.5 M mannitol solution; and (**j**–**l**) 1 M mannitol solution.

Figure 2a,d,g,j shows the series of BiOCl prepared in water and mannitol solutions in various concentrations. BiOCl_0M prepared in water was consisted of large amounts of nanosheets with a width of 0.48–1.9 µm and thickness of 50–70 nm. These nanoplates possessed rounded edges, and part of nanoplates resembled an irregular square. As shown in Figure 2d, BiOCl synthesized in the lowest concentration of mannitol contained more homogeneous and much smaller nanoplates with a width of 41.3–66.6 nm and thickness of 50–70 nm. The higher concentration of mannitol affected the BiOCl particle size. Thus, they were 13.4–25 nm and 10–15 nm for BiOCl_0.5M and BiOCl_1M, respectively. The changes in particle thickness were not observed. Similar results were obtained for BiOBr photocatalysts, except for BiOBr_1M synthesized in 1 M mannitol solution. Particles of BiOBr_1M (Figure 2k) were constructed into a flower-like microsphere of tight nanoplates with irregular edges. Our results are consistent with a previous report that mannitol can lead to the formation of hierarchical nanostructures [13]. It is worth mentioning that only

the BiOBr_1M possessed a hierarchical structure, which indicated that the interaction between the solvent and precursors was more complex and required further research.

Furthermore, BiOI synthesized in water (Figure 2b) was composed of irregular square-like nanosheets, with a low tendency to agglomerate. The nanosheets size of the BiOI series was in the range of 1.51–3.26 μm, and its thicknesses were similar to BiOCl and BiOBr. In a 0.1 M mannitol solution, a nanoparticle of BiOI agglomerated into rose-like microstructures (0.74–1.21 μm) composed of dozen thicker and smaller nanoplates (213–357 nm) than those formed in water. The concentration of mannitol higher than 0.1 M prevented agglomerations of the forming nanoplates. This fact could be related to the mannitol solution's viscosity (Table 2), which increased with increasing mannitol concentration. Additionally, nanoplates of BiOI were smaller with the increasing concentration of mannitol. This trend was also observed during the preparation of the series of BiOCl samples.

Table 2. Physicochemical properties of the mannitol solutions (Temp: 20 °C).

Type of Solution	Density [g cm^{-3}]	Viscosity [cP]
deionized water	0.99823	1.005
0.1 M mannitol	1.00383	1.087
0.5 M mannitol	1.03534	1.269
1 M mannitol	1.06681	1.763

The inhibition of the growth of BiOX (X = Cl, Br, I) nanoparticles in the mannitol solutions clearly showed that the solvent with a long chain and polyhydroxy groups was both a soft template and structure-directing agent. The significant factors that influenced BiOX nanoparticles' formation were the size and interaction of halogen ions with the solvent and the concentration of the mannitol solution. Therefore, the products' morphology can be modulated by adjusting the appropriate concentration of mannitol as a solvent.

2.1.3. XPS Analysis

The surface chemical composition and the valance state of the BiOX (X = Cl, Br, I) were characterized using X-ray photoelectron spectroscopy (XPS). The results are shown in Table 3 and Figure 3.

Table 3. The binding energy of bismuth species observed character of atoms in a surface layer of prepared photocatalysts.

Sample	BE Bi 4f $_{7/2}$ (eV)				BE Bi 4f $_{5/2}$ (eV)			
	$Bi^{(3-x)+}$	Bi^{3+}	Bi^{4+}	Bi^{5+}	$Bi^{(3-x)+}$	Bi^{3+}	Bi^{4+}	Bi^{5+}
BiOCl_0M	158.8	160.1	-	-	163.7	165.4	166.6	-
BiOCl_0.1M	158.7	159.9	161.1	-	163.6	165.2	166.4	-
BiOCl_0.5M	158.4	159.8	161.1	-	163.4	165.0	166.3	-
BiOCl_1M	158.6	160.0	161.1	-	163.6	165.3	166.5	-
BiOBr_0M	158.0	160.1	-	-	163.3	165.4	-	-
BiOBr_0.1M	158.2	159.9	160.9	-	163.2	165.2	166.1	-
BiOBr_0.5M	158.3	159.8	161.0	-	163.1	165.1	166.3	-
BiOBr_1M	158.3	159.9	160.9	-	163.6	165.2	166.2	-
BiOI_0M	-	159.4	161.5	-	-	165.0	166.6	-
BiOI_0.1M	-	159.6	161.3	162.7	-	164.8	166.6	167.7
BiOI_0.5M	-	159.9	161.1	162.5	-	165.2	166.4	167.8
BiOI_1M	-	159.9	161.0	162.5	-	165.2	166.3	167.7

"-"—absence.

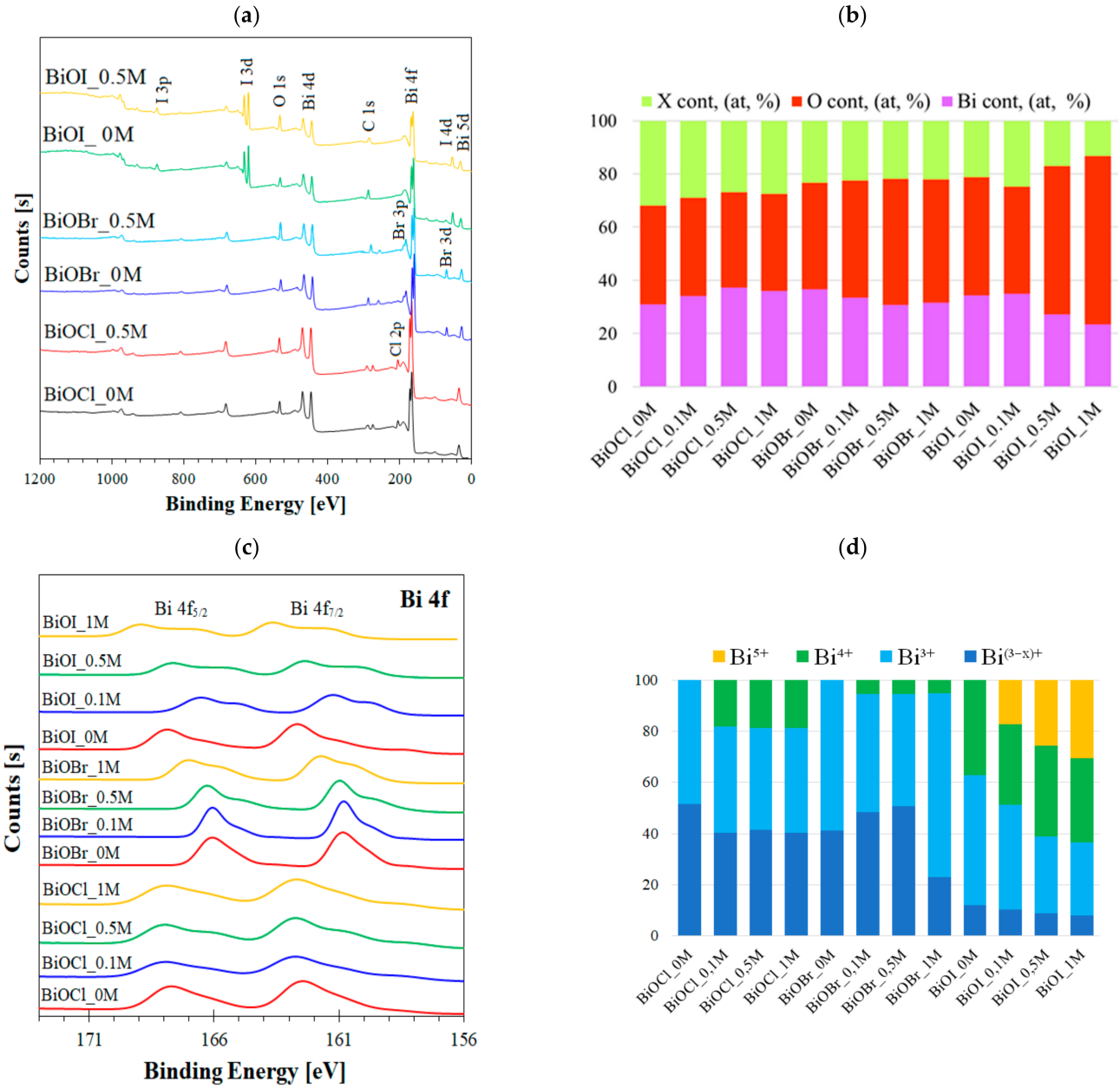

Figure 3. (**a**) Survey spectra of selected BiOX (X = Cl, Br, I); (**b**) surface elemental composition of BiOX (X = Cl, Br, I); (**c**) effect of mannitol on high-resolution spectra of Bi 4f in BiOX (X = Cl, Br, I); and (**d**) the concentration of mannitol resulting in the bismuth species ratio.

Interestingly, the Bi $4f_{5/2}$ and Bi $4f_{7/2}$ regions for BiOCl_0M and BiOBr_0M synthesized in water were fitted into the peaks attributed to Bi^{3+} and $Bi^{(3-x)+}$. This fact suggested the formation of oxygen vacancies in the samples. In the synthesis of BiOCl and BiOBr with mannitol solutions, additional new peaks appeared at the higher binding energies of 165.1 eV (±0.4 eV) and 161.1 eV (±0.4 eV). The peaks were attributed to the higher valance state of bismuth Bi^{4+}. BiOI prepared in the ultrapure water included Bi^{3+}, $Bi^{(3-x)+}$, and Bi^{4+}. The higher bismuth state appeared during the BiOI synthesis in a mannitol solution similar to BiOCl and BiOBr samples (Table 4). The higher concentration of mannitol in the synthesis of BiOI resulted in the coexistence of multiple bismuth species—Bi^{3+}, Bi^{4+}, and Bi^{5+}.

Table 4. The kinetic data for photocatalytic degradation of selected micropollutants over BiOX (X = Cl, Br, I).

Sample Label	Rh B		Cr^{6+}		5-FU	
	k_{app} [min^{-1}]	R^2	k_{app} [min^{-1}]	R^2	k_{app} [min^{-1}]	R^2
BiOCl_0M	0.152	0.9736	0.003	0.9627	0.076	0.9972
BiOCl_0.1M	0.045	0.9743	0.006	0.9703	0.008	0.9569
BiOCl_0.5M	0.084	0.9761	0.021	0.9715	0.022	0.9799
BiOCl_1M	0.070	0.9746	0.017	0.968	0.093	0.9989
BiOBr_0M	0.046	0.9667	0.001	0.9554	0.007	0.9909
BiOBr_0.1M	0.068	0.9822	0.010	0.9635	0.097	0.9521
BiOBr_0.5M	0.115	0.9977	0.022	0.9613	0.021	0.9902
BiOBr_1M	0.092	0.9986	0.025	0.9813	0.017	0.9796
BiOI_0M	0.008	0.9791	0.003	0.9782	inactive	
BiOI_0.1M	0.005	0.9387	0.004	0.9667	0.095	0.9886
BiOI_0.5M	0.021	0.9756	0.029	0.9938	inactive	
BiOI_1M	0.021	0.9700	0.012	0.9913	inactive	

In contrast to the XRD analysis, the XPS spectra did not show the characteristic peaks of metallic Bi^0 in the BiOI_0.5M and BiOI_1M samples. Therefore, it is supposed that Bi^0 was probably formed as the first step of the synthesis due to the high density and viscosity of mannitol solutions and its weak interaction with iodide anion. In the next step, BiOI was formed and covered the Bi^0 phase.

The percentages of Bi, O, X (Figure 3b) in the sample were similar to the theoretical amount in the pure phase of BiOX only in BiOCl_0M. For samples synthesized in mannitol solutions, a higher amount of oxygen than their stoichiometric amount in the BiOX crystal lattice was found. This trend was very clearly observed in the series of BiOI, where oxygen was 44.4% and 63.1% for BiOI_0M and BiOI_1M, respectively. A correlation between the oxygen amount and the number of Bi ions at a higher oxidation state in samples was also found (Figure 3b,d).

The existence of Bi^{4+} and Bi^{5+} in BiOX materials was surprising and rarely reported in the literature. Species such as Bi^{4+} and Bi^{5+} were presented in BiOBr prepared with shape controlling agent polyvinylpyrrolidone (PVP) [39] or in other bismuth-based materials (Bi_2WO_6) [40]. Bismuth at the higher oxidation state than Bi^{3+} was observed in $BiOCl_xI_{1-x}$ solid solution and was responsible for enhanced electron transfer, thus photocatalytic activity [41]. It worth mentioning that the previously reported Bi^{4+} and Bi^{5+} were generated in BiOX in a rather small amount (up to 18%). In the synthesis with surfactants, they were formed in 5.4–16.3% and 2.2–7.7% for Bi^{4+} and Bi^{5+}, respectively. In the presented study Bi^{4+} existed in 18.2–18.7%, 5.4%, and 31.4–37.3% for BiOCl, BiOBr, and BiOI, respectively. Additionally, Bi^{5+} was observed in a significant amount (17.2–30.6%) in BiOI prepared in mannitol solutions. The formation of these species was probably the result of the use of mannitol in the synthesis as Bi^{4+} was absent in BiOCl_0M and BiOBr_0M while Bi^{5+} was observed only in BiOI obtained via mannitol. Furthermore, the results indicated that coordination of Bi^{3+} ions by hydroxyl groups of mannitol played a crucial role in the formation of vacancies and ability to local electron transfer in BiOX, which could enhance the separation of photogenerated electron/hole charge pairs.

2.1.4. UV–Vis/DRS Analysis

The absorption of light by semiconductors is an important factor affecting their photocatalytic performance and is one of the key factors determining their high photocatalytic activity. The UV–Vis diffuse reflectance spectra (UV–Vis/DRS) of the series of BiOX samples are shown in Figure 4.

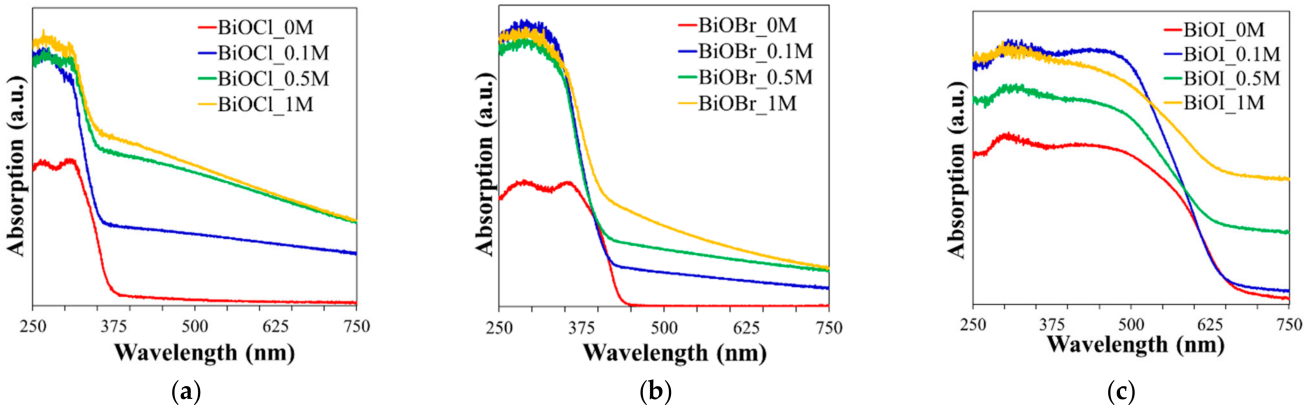

Figure 4. UV–Vis diffuse reflectance spectra of (**a**) BiOCl, (**b**) BiOBr, and (**c**) BiOI prepared with different concentrations of mannitol.

The BiOX samples of the mannitol series showed stronger absorption in the UV–Vis region compared to BiOX_0M. The increase in the concentration of the mannitol solution used for the photocatalyst preparation resulted in better absorption in the whole light range by sample due to the smaller particles and previously mentioned crystal lattice defects. With the higher mannitol concentration than 0.5 M, a slight enhancement of absorption was found. Moreover, all BiOX samples prepared in mannitol exhibited a blue-shift of absorption edges compared to BiOX obtained in water. The energy bandgap (Eg), position of maximum valance band (MVB), and minimum conduction band (MCB) were theoretically determined based on literature [18,42].

The BiOX samples of the mannitol series showed stronger absorption in the UV–Vis region compared to BiOX_0M. The increase in the concentration of the mannitol solution used for the photocatalyst preparation resulted in better absorption in the whole light range by sample. With the higher mannitol concentration than 0.5 M, a slight enhancement of absorption was found. Moreover, all BiOX samples prepared in mannitol exhibited a blue-shift of absorption edges compared to BiOX obtained in water. The energy bandgap (Eg), position of maximum valance band (MVB) and minimum conduction band (MCB) were theoretically determined based on literature [18,42] and presented in Table 3. Eg for series of BiOCl, BiOBr, and BiOI was estimated in the range of 3.0–3.3 eV, 2.56–2.65 eV, and 1.50–1.65 eV, respectively, which were consistent with the reported previously [14,23,43].

Additionally, it was observed that with increasing mannitol concentration, the bandgap of the BiOX (X = Cl, I) samples decreased, and also, the crystallite size decreased. The exception was the series of BiOBr samples, which showed a significant change in morphology (3D structure) with increasing mannitol concentration. Mannitol concentration influenced the position of the band edges Eg, as shown in Table 3. BiOX (X = Cl, Br, I) with the higher exposed facet (110) obtained in 0.5 M and 1 M mannitol characterized a lower minimum conduction band and a higher maximum valance band. The results confirmed that the appropriate synthesis conditions could offer the bang gap tuning and band-edge modification through morphology and size optimization of semiconductors.

2.1.5. PL Analysis

Photoluminescence (PL) study allowed to monitor the recombination rate of photoinduced charges pair electron-hole in the material. Figure 5 shows the PL spectra of the series of BiOCl, BiOBr, and BiOI samples excited at a wavelength of 315 nm. The emission spectra of each series had similar shapes, while the intensity of spectra decreased in the following order BiOCl > BiOBr > BiOI. This fact was related to the ability of the samples to separate e^-/h^+ charge pairs. High surface energy and reactive (001) and (110) facets found in BiOX_0M allowed for the formation of more catalytically active sits [44,45], which would explain the high intensity of the bismuth oxyhalides spectra.

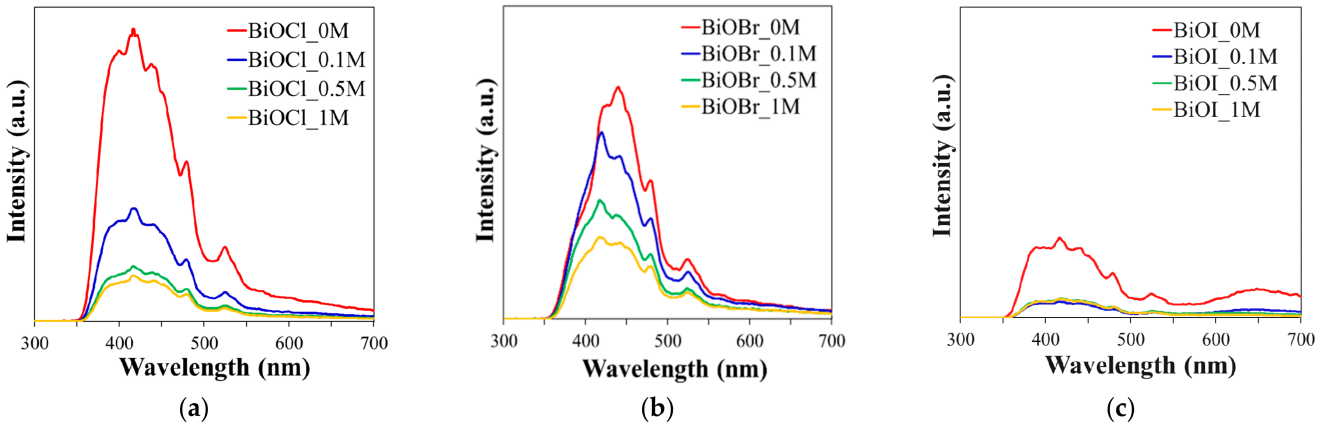

Figure 5. Photoluminescence (PL) spectra of (**a**) BiOCl, (**b**) BiOBr, and (**c**) BiOI synthesized in various concentrations of mannitol solution.

The intensity of PL spectra decreased after the introduction of mannitol to synthesize BiOX (X = Cl, Br, I) samples. Increasing the mannitol concentration decreased the PL intensity of the samples obtained in their solutions. This fact could indicate a better separation of photoexcited electron-hole pairs in these samples. The better separation of charge pairs in samples prepared in mannitol solutions was a result of (a) reduction in the size of the photocatalyst particles, (b) the appearance of highly reactive (110) facets [45], and (c) the existence of highly oxidized bismuth ions.

2.2. Photocatalytic Activity

Many factors, including morphology, crystallinity, or effective generation and separation of photoexcited charge pairs, play an essential role in influencing the efficiency of photodegradation of pollutants. Micropollutants such as Rhodamine B (RhB) cation dye, colorless cytostatic drug 5-FU, and heavy metal Cr(VI) in the form of anion form $Cr_2O_7^{2-}$ were selected for photodegradation study to examine the activity of BiOX photocatalysts. Direct and indirect photolysis of 5-FU and Cr(VI) was almost negligible, while RhB degraded by 16%, as was reported before [16].

The photocatalytic activities of the three series of BiOX (X = Cl or Br or I) in the photooxidation of RhB were conducted, and the results are shown in Figure 6. The pseudo-first-order rate constants k_{app} were calculated, and the results are presented in Table 4.

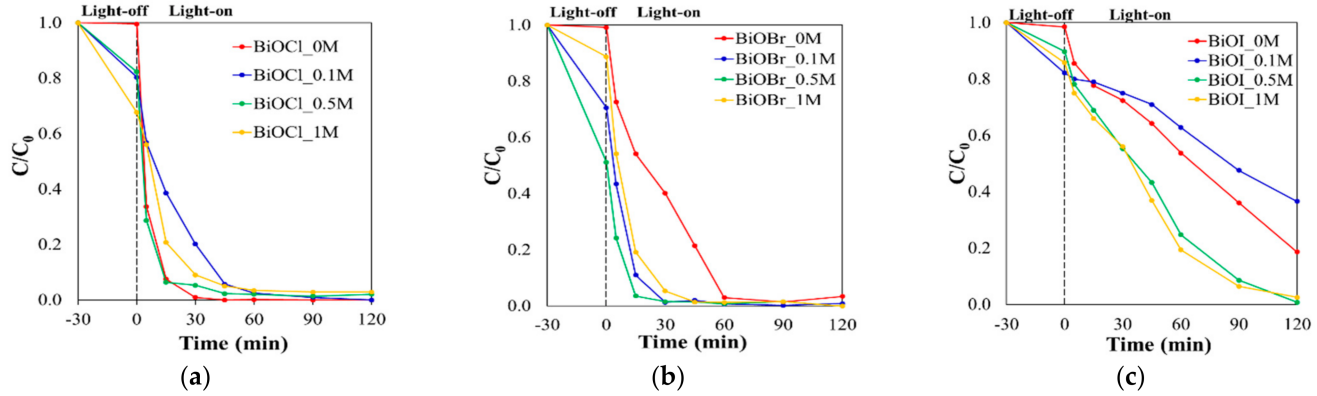

Figure 6. Photocatalytic degradation of RhB over (**a**) BiOCl, (**b**) BiOBr, and (**c**) BiOI under UV–Vis irradiation.

Regardless of the type of halogen in BiOX prepared in distilled water (BiOX_0M), the adsorption of RhB on the photocatalyst surface was not observed. Similar results for high crystallinity nanoplates BiOX were reported by other groups [6,15]. However, with the increase of mannitol concentration used in BiOX synthesis from 0.1 M to 1.0 M, the dye

adsorption efficiency elevated. The trend for all prepared series was observed, but the largest increase in RhB absorption for the BiOBr samples was found. The adsorption of this dye reached the highest value of 49% for the BiOBr_0.5M photocatalyst. The adsorption of RhB was related instead to morphology changes than the $Bi^{(3-x)+}$, Bi^{4+}, and Bi^{5+} bismuth species in the crystal lattice.

The value of pseudo-first-order kinetic rate constant k_{app} of RhB photooxidation in the series of BiOCl was the highest for BiOCl_0M, while in the series of BiOBr and BiOI, the highest value of k_{app} was obtained for the samples prepared in 0.5 M mannitol solution.

In the literature, the photocatalyst activity in RhB oxidation was correlated with the structure of the prepared samples. Furthermore, density functional theory (DFT) computations showed a strong relationship with the importance of existence (001), (010), and (110) facets in BiOX and their photocatalytic activity [44,46].

The (001) plane with high thermodynamic stability has been previously reported as beneficial to photocatalytic performance, including RhB oxidation [46]. The remarkable photocatalytic degradation of RhB was observed over irradiation of the dye in the presence of BiOCl_0M, which possessed well-formed, exposed {001} planes. The samples prepared in mannitol solutions were characterized by a decrease in {001} planes with an increase in the mannitol concentration used in the synthesis. Therefore, the RhB removal rate was lower for BiOCl samples prepared in mannitol solutions.

Decomposition in the presence of BiOBr_0M with well-developed (002), (003), and (004) planes showed the lowest activity in series of BiOBr samples, which suggested that exposed facets were a minor factor in the photocatalytic oxidation of RhB in this series. Noticeably, the BiOX_0.5M (X = Br, I) with small uniform nanosheets and well exposed (110) crystal face exhibited the highest photocatalytic activity among the samples prepared in mannitol solutions. Therefore, the (110) crystal face with a higher electron density seems to be more critical to photocatalytic oxidation of RhB. The higher (110) active facet exposure found for BiOBr_0.5M allowed separate free electrons more effectively and enhanced the photocatalytic activity compared with other BiOBr samples. The previous research has indicated that the exposed (110) crystal plane facilitated the migration of oxidants holes and reduced the recombination of photogenerated electron-hole pairs in the BiOBr [35]. A similar trend was found for the series of BiOI.

Moreover, the analysis of the O/X ratio, where X = Cl, Br, I, and Bi described in the XPS results showed that the photodegradation efficiency of RhB gradually increased with the increase in the amount of oxygen in the semiconductors. That was probably the result of better separation of e^-/h^+ pairs and the effective mobility of holes due to defects in the samples.

The difference in the activity trend of the series of BiOCl and BiOBr/BiOI could be related to another phenomenon. RhB molecules could behave as photosensitizers, absorb light energy and convert into an excited state (RhB*). The excited state could inject electrons into the CB of the photocatalyst, trapped by dissolved O_2 in solution to generated oxidizing species such as superoxide radicals. The photocatalytic oxidation occurred between these active species and RhB^+. The following reactions to achieve the aim of degradation were possible (Equations (1)–(3)):

$$RhB + h\nu \rightarrow RhB^* \quad (1)$$

$$RhB^* + BiOX \rightarrow BiOX/\ e^- + RhB^{+\bullet} \quad (2)$$

$$RhB^{+\bullet} + {O_2}^{-\bullet} \rightarrow \text{by-products} \rightarrow H_2O + CO_2 \quad (3)$$

The synthesis of BiOX (X = Cl, Br, I) in mannitol solution favored surface creation and (110) facet exposition; thus, photoexcited electrons could have a lower recombination rate. Therefore, more electrons were trapped by the dissolved oxygen, and more $^{\bullet}O_2^-$ could be produced. The increase in superoxide radical's production is beneficial for RhB degradation. Therefore, this phenomenon can explain the higher activity toward RhB oxidation of the samples prepared in mannitol.

It is worth mentioning that the samples obtained by us in mannitol solution compare to the BiOX (X = Cl, Br, I) photocatalyst prepared via surfactants: hexadecyl(trimethyl)ammonium bromide (CTAB) [35,47,48], PVP [39], or sodium dodecyl sulfate (SDS) [39] reported in literature showed remarkable higher photocatalytic performance toward RhB oxidation.

To demonstrate the potential application of the presented BiOX materials in the oxidation of pharmaceuticals, the cytostatic drug 5-FU was used as a model compound. In contrast to RhB, 5-FU characterized the low partition coefficient $K_{o/w}$. The results of the 5-FU photocatalytic oxidation are shown in Figure 7.

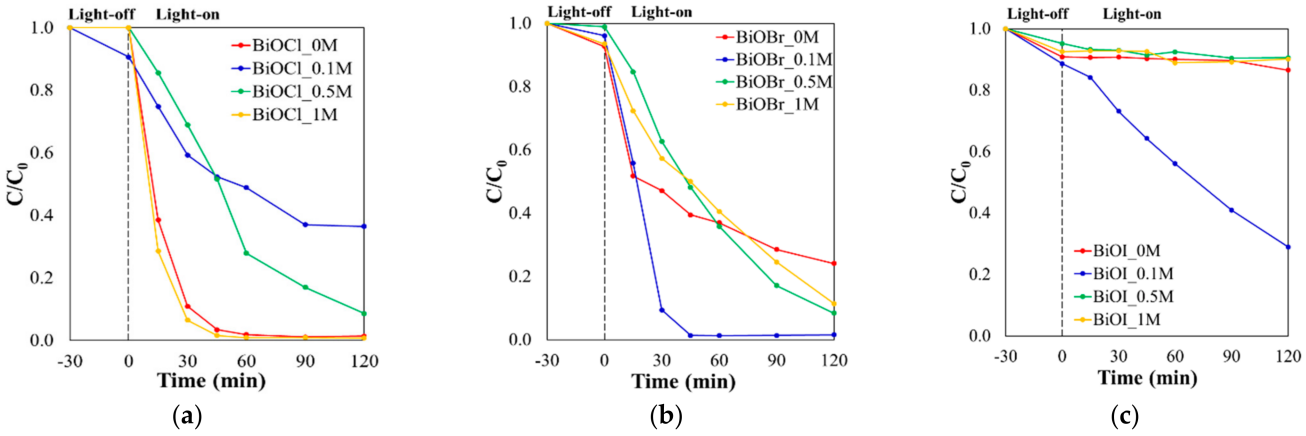

Figure 7. Photocatalytic degradation of 5-fluorouracil in the presence of (**a**) BiOCl, (**b**) BiOBr, and (**c**) BiOI under UV–Vis irradiation.

Previous studies have proved that mainly holes (h^+) were involved in the oxidation of 5-FU using BiOX photocatalysts, while superoxide radicals [17] were the minor oxidant of this drug. All prepared BiOX samples exhibited low 5-FU adsorption on their surface, and the highest values were 12%, 10%, and 10% for BiOI_0.1M, BiOCl_0.1M, and BiOI_0M, respectively. The pseudo-first-order rate constants k_{app} were calculated, and the results are listed in Table 5.

Table 5. Sample label of studied BiOX.

No.	Sample Label	BiOX Precursors	Solvent
Bismuth oxychloride			
1.	BiOCl_0M	2 mmol KCl, 2 mmol $Bi(NO_3)_3{\cdot}5H_2O$	deionized water
2.	BiOCl_0.1M		0.1 M mannitol
3.	BiOCl_0.5M		0.5 M mannitol
4.	BiOCl_1M		1 M mannitol
Bismuth oxybromide			
5.	BiOBr_0M	2 mmol KBr, 2 mmol $Bi(NO_3)_3{\cdot}5H_2O$	deionized water
6.	BiOBr_0.1M		0.1 M mannitol
7.	BiOBr_0.5M		0.5 M mannitol
8.	BiOBr_1M		1 M mannitol
Bismuth oxyiodide			
9.	BiOI_0M	2 mmol KI, 2 mmol $Bi(NO_3)_3{\cdot}5H_2O$	deionized water
10.	BiOI_0.1M		0.1 M mannitol
11.	BiOI_0.5M		0.5 M mannitol
12.	BiOI_1M		1 M mannitol

The sample BiOCl_0M showed remarkable photocatalytic activity toward oxidation 5-FU (k_{app} = 0.076 min^{-1}). However, in the series of BiOCl, BiOCl_1M obtained in 1 M mannitol solution exhibited the highest degradability of 5-FU. After 45 min of irradiation,

almost 100% of the drug was decomposed with the k_{app} of 0.093 min^{-1}. Preparation of BiOCl_0M in water resulted in the formation of many active sites, which allowed for the generation of charge carriers e^-/h^+, which was observed as a high intensity of PL spectra. The enhancement of BiOCl_1M activity could be attributed to both the diminishing and unifying of nanoplates and the creation of surface defects. These occurrences prolonged the life of photoexcited holes and increased the 5-FU removal rate. A similar result was reported for the 3D flower-like BiOCl obtained in glycerol [17]. The authors also explained the photocatalyst's high activity in the 5-FU decomposition by the long lifetime of holes. Due to the drug's low affinity to the BiOX surfaces, this factor was crucial for 5-FU decomposition with success. Mannitol solution used for the synthesis of BiOX regulated their morphologies and surface structures resulted in an enhanced degradation efficiency of selected micropollutants.

The BiOBr_0.1M sample prepared in 0.1 M mannitol solution exhibited the best photocatalytic activity toward 5-FU (k_{app} = 0.097 min^{-1}) in series of BiOBr. The efficiency removal of the drug, using BiOBr_0.1M, reached 91% after 30 min of UV–Vis irradiation, while for the remaining samples, it was in the range from 18% to 53%. The increase in activity of BiOBr_0.1M toward 5-FU degradation was probably related to the higher I_{110}/I_{102} ratio and the exposure of the (110) facet responsible for the reduction and generation of superoxide radicals. As it was discussed above, superoxide radicals could participate in the decomposition of 5-FU. Moreover, the contribution of surface defects in BiOBr_0.1M sample was 48.5% of $Bi^{(3-x)+}$ and 5.4% Bi^{4+}. Their existence in the photocatalyst slowed down the recombination of photogenerated charge pairs and enhanced the degradation rate of 5-FU. Compared to our previously reported $Bi_4O_5Br_2$ [16] and $BiOCl_{0.5}Br_{0.5}$ [17], the presented BiOBr prepared in a 0.1 M mannitol solution showed higher 5-FU photodegradation ability. The results indicated a crucial role of mannitol as a capping agent during BiOX synthesis.

The prepared series of BiOI exhibited much lower photocatalytic activity than BiOCl and BiOBr, which was connected to its narrower energy bandgap. The main factor influence activity toward 5-FU degradation was morphology, and surface defects prevented from the recombination of photogenerated holes and electrons in BiOI [47]. Only BiOI_0.1M with 3D rose-like microspheres decomposed 5-FU, and after 120 min of irradiation, 71% of the drug was removed at the k_{app} of 0.095 min^{-1}. BiOI synthesized in this work is characterized by the higher degradation rate of 5-FU than $Bi_4O_5I_2$ prepared via ionic liquids reported by our research group [16]. It is believed that $Bi_4O_5I_2$ has a stronger redox ability than BiOI [49,50]. However, the results implying the beneficial influence of mannitol on the redox potential of holes photogenerated under irradiated BiOI. The same trend was found in BiOCl and BiOBr materials.

The influence of mannitol concentration on the prepared samples' photoreduction ability was the next step of our investigations. Figure 8 shows Cr(VI) photoreduction activities under UV–Vis light on BiOX (X = Cl, Br, I).

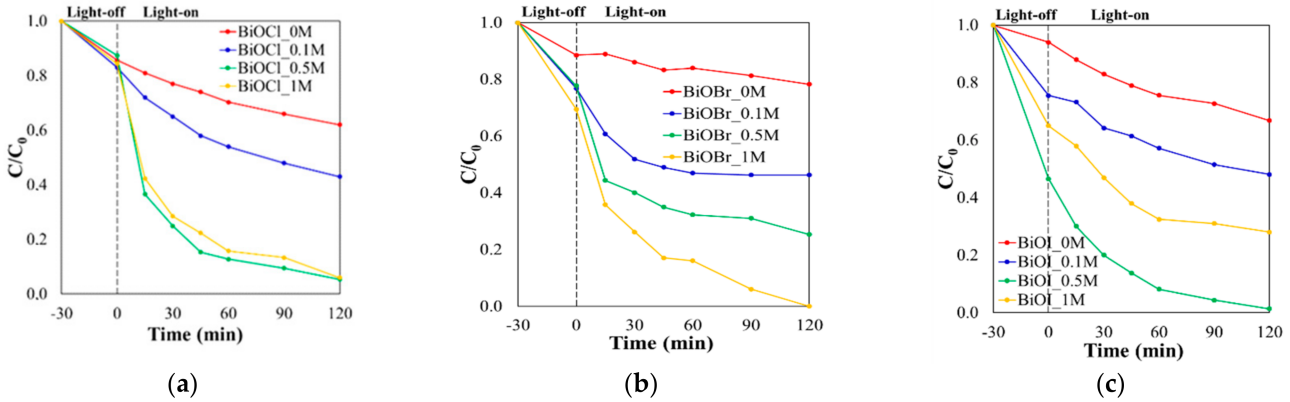

Figure 8. Photocatalytic reduction of hexavalent chromium over (**a**) BiOCl, (**b**) BiOBr, and (**c**) BiOI under UV–Vis irradiation.

The adsorption of Cr(VI) in the form of $Cr_2O_7^{2-}$ ions increased in the following order BiOCl < BiOBr < BiOI. Moreover, the adsorption efficiency of Cr(VI) ions increased with the elevation of mannitol concentration used for the BiOX synthesis. Defects such as Bi^{4+} and Bi^{5+} in the crystal lattice resulted in a higher positive charge of BiOX surfaces. Their number in the sample increased with the increase in the concentration of mannitol used for synthesis. The photocatalyst surface's positive charge was favorable for $Cr_2O_7^{2-}$ ions adsorption due to their electrostatic interaction.

In Table 5, the pseudo-first-order kinetic rate constant k_{app}, calculated based on the results, are presented. BiOCl_0.5M and BiOCl_1M gave much higher activity in Cr(VI) reduction than BiOCl_0M and BiOCl_0.1M. The efficiency of reduction of Cr(VI) reached 38%, 57%, 95% and 94% for BiOCl_0M, BiOCl_0.1M, BiOCl_0.5M and BiOCl_1M, respectively.

The series of BiOBr exhibited a higher degradation rate among the prepared BiOX, which increased from 0.001 min^{-1} (BiOBr_0M) to 0.025 min^{-1} (BiOBr_1M) with an increasing concentration of mannitol used in the synthesis. Among BiOBr samples, BiOBr_1M showed the highest rate and efficiency of Cr(VI) removal. Photoreduction of Cr(VI) in the form of $Cr_2O_7^{2-}$ increased with an increase in the concentration of mannitol used in the synthesis and resulted in 22%, 54%, 75%, and 100% degradation after 120 min in the presence of BiOBr_0M, BiOBr_0.1M, BiOBr_0.5M and BiOBr_1M, respectively.

The photocatalytic activity toward Cr(VI) among BiOI samples increased with increasing mannitol concentration used for synthesis up to 0.5M, and BiOI_0.5M exhibited the highest value of k_{app}. For 1 M mannitol concentration, the k_{app} decreased. The Cr(VI) in the solution was degraded in 32%, 52%, 99%, and 72% after 120 min of illumination over BiOI_0M, BiOI_0.1M, BiOI_0.5M, and BiOI_1M, respectively.

The results suggested that Cr(VI) reduction was facet dependent, and materials with dominated the (110) facet exhibited higher efficiency in its reduction. BiOX photocatalysts prepared in mannitol solutions were characterized by many exposed (110) crystal planes. The same trend was reported for BiOBr [51]. The number of exposed (110) crystalline planes in the sample correlated with Cr(VI) reduction activity. However, BiOX with many exposed (110) crystal planes was previously synthesized with PVP as a structure-directing agent [35]. BiOX with exposed (110) crystal planes was prepared in a less expensive and environmentally friendly mannitol solution in our study. The presence of mannitol in the synthesis affected the I_{110}/I_{102} ratio in the BiOX samples, which are summarized in Table 5. The exposure of (110) facets and value of the I_{110}/I_{102} ratio increased with the mannitol concentration in the series of BiOCl and BiOBr. In the series of BiOI, the activity of BiOI_0.5M and BiOI_1M in the Cr(VI) reduction process was inhibited.

Nevertheless, the XRD analysis showed that BiOI samples prepared in mannitol solutions possessed an additional metallic bismuth phase in a crystalline lattice, which could prolong photogenerated charge pairs' lifetime through separation acted as a sink for electrons and enhanced oxidation processes. However, in the photoreduction of $Cr_2O_7^{2-}$ ions, the excited electrons were the main species, and the presence of Bi^0 prevented reaction between electrons and Cr(VI) ions. The lower photocatalytic activity of BiOI_1M than BiOI_0.5M could be explained by the higher content of the metallic bismuth phase that participated in the photoreduction of chromium (VI).

Additionally, the enhanced photoreduction of Cr(VI) in the presence of irradiated BiOX could be attributed to the strong adsorption on the photocatalyst's surface, which was obtained by the use of mannitol for synthesis. The previously reported surfactants addition to the BiOX synthesis [35,52] and BiOX modifications [53] did not elevate the Cr(VI) adsorption on the photocatalyst surface to such an extent. Based on the results obtained, it could be concluded that the mannitol used in the synthesis as a template and capping agent played a crucial role in the exposure of (110) plane of BiOX (X = Cl, Br, I) and the creation of defects. These phenomena enhanced the adsorption and reduction of $Cr_2O_7^{2-}$ ions.

The obtained results indicated that the photocatalytic activity of BiOX (X = Cl, Br, I) was closely related to the presence of mannitol at a particular concentration, which was

used in the synthesis process due to its dual roles in the morphology regulation and the surface defects creation.

2.3. Mechanism of BiOX Crystallites Formation

The processes for the formation of BiOX crystallites in mannitol solutions could be described by the following chemical equations (Equations (4)–(6)):

$$2Bi^{3+} + 2C_6H_8(OH)_6 \rightarrow Bi_2(C_6H_8O_6) + C_6H_8(OH_2)_6{}^{6+} \quad (4)$$

$$Bi_2(C_6H_8O_6) + 2X^- + 2H_2O \rightarrow 2BiOX_{(s)} + C_6H_8O_6{}^{6-} + 4H^+ \quad (5)$$

$$C_6H_8O_6{}^{6-} + C_6H_8(OH_2)_6{}^{6+} \rightarrow 2C_6H_8(OH)_6 \quad (6)$$

The proposed formation mechanism is presented in Figure 9.

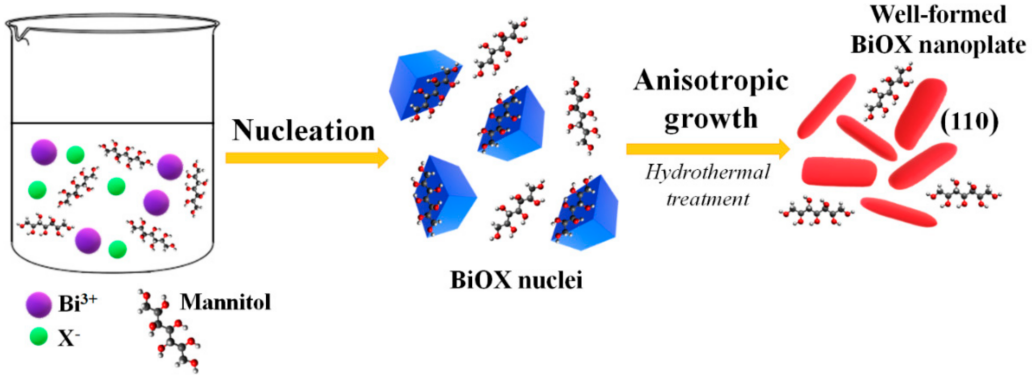

Figure 9. The illustration of the formation mechanism of BiOX mannitol-assisted hydrothermal treatment.

Mannitol with polyhydroxy structure mediated the nucleation and crystal growth of BiOX nanoparticles by creating the multi-dental bismuth ligand ($Bi_2(C_6H_8O_6)$) with strong interactions with Bi^{3+} ions. The viscosity and density of the 0.1 M mannitol solution were higher than that of H_2O, and these parameters increased with the elevation of mannitol concentration (Table 2). Therefore, the rate of halide ions diffusion was successively inhibited by elevation of mannitol concentration from 0.1 M to 1 M. Moreover, the halides' diffusion rate in the mannitol solution decreased with the increase of the anion radius ($Cl^- < Br^- < I^-$). The reaction rate between the two Bi^{3+} ions coordinated by one molecule of mannitol (bismuth alkoxide) with six ions of iodide in a 0.5 M concentration of mannitol was probably so low that reduction of Bi^{3+} by mannitol to metallic Bi^0 was observed. This phenomenon led to metallic bismuth formation during the preparation of BiOI_0.5M and BiOI_1M samples. The bismuth alkoxides could decompose during solvothermal treatment associated with high temperature and pressure, mainly to BiO^+. The forming metal-ligand complex and its slow decomposition at high concentration of mannitol, low availability of Bi^{3+}, and slow diffusion rate of halide ions, resulted in oxygen-rich BiOX Bi^{4+}/Bi^{5+} species. A higher amount of these species was reached in the BiOI samples obtained in the synthesis with me^- ions characterized by the largest radius of ion among halides.

Moreover, the mannitol concentration's increased viscosity significantly suppressed the nanocrystals' intrinsic anisotropic growth, as was confirmed by the SEM images. The results suggested that the nucleating speed could be controlled by the mannitol's density and viscosity, which is beneficial for nanosheets formation. Additionally, the higher concentration of mannitol prevents the aggregation of nanoparticles. The surface energy of the BiOBr nanosheets prepared in 1 M mannitol was too high; therefore, it aggregated into the hierarchical structure for the surface energy reduction. Moreover, in the solvothermal reaction, $C_6H_8O_6{}^{6-}$ was the by-product (Equation (5)) that could be easily adsorbed on the exposed Bi^{3+} (102) facets and favors formation {110} planes. Mannitol also limited the

anisotropic crystal growth along the [001] direction due to repulsion of $C_6H_8O_6^{6-}$ and terminal oxygen of (001) facets.

In summary, mannitol acted as a structure-directing agent and a growth and shape control agent. The existence of electrostatic attraction and hydrogen bonds between mannitol molecules and the long carbon chain helped form a uniform nanosheet (BiOCl, BiOBr, and BiOI) or 3D flower-like heterostructure (BiOBr).

3. Materials and Methods

Bismuth nitrate, potassium chloride, potassium iodide, mannitol, sulphuric acid, acetone, and potassium dichromate were purchased from StanLab Sp. J. (STANLAB, Lublin, Poland). Potassium bromide was obtained from Alfa Aesar (Alfa Aesar, Karlsruhe, Germany). Ethyl alcohol, 1,5-diphenylcarbazide, and rhodamine B were purchased from POCh S.A. (POCH S.A. Gliwice, Poland). The drug 5-fluorouracil was obtained from Sigma-Aldrich (St. Louis, MO, USA). Orthophosphoric acid was provided by Chempur (Piekary Śląskie, Poland). All chemicals used in this study were commercially available analytical grade and were used without further purification.

3.1. Synthesis

The series of BiOX (X = Cl, Br, I) semiconductors were prepared by a solvothermal method. Briefly, 2 mmol of KX (X = Cl, Br, I) were dissolved in 20 mL of deionized water or mannitol solution, and 2 mmol of $Bi(NO_3)_3{\cdot}5H_2O$ were suspended by sonification for 15 min. The KX solution was then added dropwise to 20 mL of deionized water containing bismuth nitrate suspension under vigorous stirring. After 30 min continuously stirring, the mixture was transformed into a 50 mL Teflon-lined stainless-steel autoclave. Then the autoclave was sealed and heated at 160 °C for 16 h. After heat treatment, the autoclave was allowed to cool naturally to room temperature. The products were collected and washed with ethanol and deionized water thoroughly and dried at 80 °C. The series of BiOX was synthesized using various concentrations of mannitol, i.e., 0.1 M, 0.5 M, and 1 M. The list of prepared photocatalysts is presented in Table 1. The density of mannitol solutions was measured by the picometric method, and the viscosity was determined with the Ostwald viscometer. The obtained results are summarized in Table 5.

3.2. Characterization

The crystalline phase and the prepared photocatalysts' purity were characterized by X-ray powder diffraction on a D2 Phaser (Bruker, Billerica, MA, USA). Diffraction patterns were taken over the 2θ in the range 20–70°. X-ray photoelectron spectroscopy with ThermoFisher Scientific Escalab 250Xi (Waltham, MA, USA) was used to determine the chemical state of the elements and the composition of the surface of the BiOX. The morphology of the products was characterized by a field-emission scanning microscope (JEOL JSM-7610F FEG SEM), (JEOL Ltd., Akishima, Japan). UV–Vis diffuse reflectance spectra were recorded on a UV-2600 UV–VIS Spectrometer (Shimadzu Corp., Kyoto, Japan) using $BaSO_4$ as a reference. Photoluminescence spectra were measured on Perkin Elmer limited LS50B (Perkin Elmer, Waltham, MA, USA) using 315 nm as an excitation wavelength.

3.3. Photocatalytic Activity

The photocatalytic activity was evaluated by degradation of RhB dye, hexavalent chromium anion in the form of $Cr_2O_7^{2-}$ and cytostatic drug 5-FU. The concentration of RhB, 5-FU was 15 mgL^{-1} at pH 6.5, and Cr(VI) was 20 mgL^{-1} at pH 3. The concentration of photocatalysts during RhB and 5-FU degradation was 0.2 gL^{-1}, and Cr(VI) was photoreduced in the presence of 0.5g L^{-1} photocatalyst. The volume of the solution in the tests was 15 mL. Photocatalytic degradation experiments were conducted as follows: the photocatalyst was immersed in a selected micropollutant solution and magnetically stirred in the dark for 30 min to achieve the predetermined adsorption–desorption equilibrium; then, the solution was exposed to UV–Vis light irradiation of 150 W medium pressure

mercury lamp for 120 min. At particularly time intervals, 1 mL of samples were collected, and the photocatalysts particles were removed immediately. The concentration of RhB was analyzed with a Perkin Elmer Lambda XLS+ spectrophotometer by monitoring the absorption peak at 553 nm. The Cr(VI) concentration was determined according to ISO PN-EN 18412. The 5-FU degradation was measured by HPLC analysis using Perkin Elmer Series 200 equipped with UV detector and Phenomenex C-18 column (150 mm × 4.6 nm, 2.6 μm) with parameters as follows: detection wavelength of 266 nm, the mobile phase was acetonitrile/water 2:98 (*v*/*v*), the retention time (t_R) was 4.9 min. The experiments were repeated three times, and the accuracy expressed as the relative standard deviation of three independent measurements did not exceed 3%. The sorption test was conducted in the dark for 120 min and revealed that after 30 min, the adsorption–desorption equilibrium was achieved for selected micropollutants and prepared BiOX.

4. Conclusions

In this study, a series of BiOX (X = Cl, Br, I) photocatalysts via a solvothermal process in mannitol solution were fabricated. It was found that the role of mannitol was strongly dependent on its concentration (in the range of 0–1 M). The mannitol solution's viscosity and density played a crucial role in the phase composition, morphology, and surface defect formation of the obtained photocatalysts. Mannitol simultaneously could act as a solvent, soft template, and structure-directing agent in the synthesis of BiOX (X = Cl, Br, I). The mannitol concentration affected particles' size; the higher its concentration, the smaller and more unified nanoparticles were formed. The presence of polyxydroksyl alcohol in the synthesis of BiOX had a high impact on the (110) and (102) facets growth, and the I_{110}/I_{102} ratios increased as the mannitol concentration increased.

Moreover, the photocatalysts synthesized in mannitol solutions characterized the prolonged life of pair charge carriers e^-/h^+ caused due to the appearance of surface defects ($Bi^{(3-x)+}$, Bi^{4+}, and Bi^{5+}). The defects with positive charge were responsible for the higher adsorption of negatively charged ions $Cr_2O_7^{2-}$, and RhB with aromatic rings. The increase in photocatalytic rate and performance toward the RhB, 5-FU, and Cr(VI) removal resulted from the higher adsorption ability and better separation of e^-/h^+ charge carriers. The photocatalytic degradation toward RhB, 5-FU, and Cr(VI) over the prepared BiOX was followed as a pseudo-first-order kinetic model.

Among all studied samples, BiOCl_0M and BiOBr_0.5M exhibited the best activity toward RhB. Based on the degradation rate of Rhodamine B, the optimal concentration of the mannitol solution used in the BiOI synthesis was 0.5M. The BiOX prepared in 0.5M mannitol solution, regardless of halogen, showed the highest efficiency of Cr(VI) removal under UV–Vis irradiation. Moreover, comparing the photocatalytic activities of the BiOCl, BiOBr, and BiOI series, it was found that the optimal mannitol concentration used in the preparation of the material were 1 M, 0.1 M, and 0.1 M for BiOCl, BiOBr, and BiOI, respectively. The possible mechanism of crystal growth has been proposed.

Mannitol is a simple and environmentally friendly compound. Our presented studies demonstrated that BiOX prepared in mannitol solution could be useful for efficiently removing a wide range of micropollutants.

Author Contributions: Conceptualization, A.B.-G., P.W., and E.M.S.; methodology, A.B.-G. and P.W.; validation, P.W. and A.B.-G.; formal analysis, P.W., A.B.-G., and E.M.S.; investigation, A.B.-G., P.W., K.S., A.M., J.R., and K.T.; resources, A.B.-G. and E.M.S.; data curation, A.B.-G.; writing—original draft preparation, A.B.-G., P.W., and E.M.S.; writing—review and editing, A.B.-G., P.W., and E.M.S.; visualization, P.W. and A.B.-G.; supervision, E.M.S.; project administration and funding acquisition, A.B.-G. and E.M.S. All authors have read and agreed to the published version of the manuscript.

Funding: This research was funded by the National Science Center (PL), grant number DEC-2017/01/X/ST5/01136, and the Ministry of Education and Science (PL), grant number DS 531-T020-D596-21.

Data Availability Statement: Data is contained within the article.

Conflicts of Interest: The authors declare no conflict of interest.

References

1. Ye, L.; Su, Y.; Jin, X.; Xie, H.; Zhang, C. Recent Advances in BiOX (X = Cl, Br and I) Photocatalysts: Synthesis, Modification, Facet Effects and Mechanisms. *Environ. Sci. Nano* **2014**, *1*, 90. [CrossRef]
2. Yang, Y.; Zhang, C.; Lai, C.; Zeng, G.; Huang, D.; Cheng, M.; Wang, J.; Chen, F.; Zhou, C.; Xiong, W. BiOX (X = Cl, Br, I) Photocatalytic Nanomaterials: Applications for Fuels and Environmental Management. *Adv. Colloid Interface Sci.* **2018**, *254*, 76–93. [CrossRef]
3. Liu, Y.; Hu, Z.; Yu, J. Fe Enhanced Visible-Light-Driven Nitrogen Fixation on BiOBr Nanosheets. *Chem. Mater.* **2020**, *32*, 1488–1494. [CrossRef]
4. Wu, S.; Wang, C.; Cui, Y.; Wang, T.; Huang, B.; Zhang, X.; Qin, X.; Brault, P. Synthesis and Photocatalytic Properties of BiOCl Nanowire Arrays. *Mater. Lett.* **2010**, *64*, 115–118. [CrossRef]
5. Mi, Y.; Li, H.; Zhang, Y.; Du, N.; Hou, W. Synthesis and Photocatalytic Activity of BiOBr Nanosheets with Tunable Crystal Facets and Sizes. *Catal. Sci. Technol.* **2018**, *8*, 2588–2597. [CrossRef]
6. Gao, M.; Zhang, D.; Pu, X.; Li, H.; Lv, D.; Zhang, B.; Shao, X. Facile Hydrothermal Synthesis of Bi/BiOBr Composites with Enhanced Visible-Light Photocatalytic Activities for the Degradation of Rhodamine B. *Sep. Purif. Technol.* **2015**, *154*, 211–216. [CrossRef]
7. Cheng, G.; Xiong, J.; Stadler, F.J. Facile Template-Free and Fast Refluxing Synthesis of 3D Desertrose-like BiOCl Nanoarchitectures with Superior Photocatalytic Activity. *New J. Chem.* **2013**, *37*, 3207. [CrossRef]
8. Wang, D.-H.; Gao, G.-Q.; Zhang, Y.-W.; Zhou, L.-S.; Xu, A.-W.; Chen, W. Nanosheet-Constructed Porous BiOCl with Dominant {001} Facets for Superior Photosensitized Degradation. *Nanoscale* **2012**, *4*, 7780. [CrossRef]
9. Zhang, D.; Li, J.; Wang, Q.; Wu, Q. High {001} Facets Dominated BiOBr Lamellas: Facile Hydrolysis Preparation and Selective Visible-Light Photocatalytic Activity. *J. Mater. Chem. A* **2013**, *1*, 8622. [CrossRef]
10. Hou, L.; Niu, Y.; Yang, F.; Ge, F.; Yuan, C. Facile Solvothermal Synthesis of Hollow BiOBr Submicrospheres with Enhanced Visible-Light-Responsive Photocatalytic Performance. *J. Anal. Methods Chem.* **2020**, 3058621. [CrossRef] [PubMed]
11. Hu, X.; Xu, Y.; Zhu, H.; Hua, F.; Zhu, S. Controllable Hydrothermal Synthesis of BiOCl Nanoplates with High Exposed {001} Facets. *Mater. Sci. Semicond. Process.* **2016**, *41*, 12–16. [CrossRef]
12. Jia, M.; Hu, X.; Wang, S.; Huang, Y.; Song, L. Photocatalytic Properties of Hierarchical BiOXs Obtained via an Ethanol-Assisted Solvothermal Process. *J. Environ. Sci.* **2015**, *35*, 172–180. [CrossRef] [PubMed]
13. Tian, F.; Xiong, J.; Zhao, H.; Liu, Y.; Xiao, S.; Chen, R. Mannitol-Assisted Solvothermal Synthesis of BiOCl Hierarchical Nanostructures and Their Mixed Organic Dye Adsorption Capacities. *CrystEngComm* **2014**, *16*, 4298–4305. [CrossRef]
14. Xiong, J.; Cheng, G.; Qin, F.; Wang, R.; Sun, H.; Chen, R. Tunable BiOCl Hierarchical Nanostructures for High-Efficient Photocatalysis under Visible Light Irradiation. *Chem. Eng. J.* **2013**, *220*, 228–236. [CrossRef]
15. Xiong, J.; Cheng, G.; Li, G.; Qin, F.; Chen, R. Well-Crystallized Square-like 2D BiOCl Nanoplates: Mannitol-Assisted Hydrothermal Synthesis and Improved Visible-Light-Driven Photocatalytic Performance. *RSC Adv.* **2011**, *1*, 1542. [CrossRef]
16. Bielicka–Giełdoń, A.; Wilczewska, P.; Malankowska, A.; Szczodrowski, K.; Ryl, J.; Zielińska-Jurek, A.; Siedlecka, E.M. Morphology, Surface Properties and Photocatalytic Activity of the Bismuth Oxyhalides Semiconductors Prepared by Ionic Liquid Assisted Solvothermal Method. *Sep. Purif. Technol.* **2019**, *217*, 164–173. [CrossRef]
17. Wilczewska, P.; Bielicka-Giełdoń, A.; Borzyszkowska, A.F.; Ryl, J.; Klimczuk, T.; Siedlecka, E.M. Photocatalytic Activity of Solvothermal Prepared BiOClBr with Imidazolium Ionic Liquids as a Halogen Sources in Cytostatic Drugs Removal. *J. Photochem. Photobiol. A Chem.* **2019**, *382*, 111932. [CrossRef]
18. Hao, H.-Y.; Xu, Y.-Y.; Liu, P.; Zhang, G.-Y. BiOCl Nanostructures with Different Morphologies: Tunable Synthesis and Visible-Light-Driven Photocatalytic Properties. *Chin. Chem. Lett.* **2015**, *26*, 133–136. [CrossRef]
19. Li, X.; Zhu, C.; Song, Y.; Du, D.; Lin, Y. Solvent Co-Mediated Synthesis of Ultrathin BiOCl Nanosheets with Highly Efficient Visible-Light Photocatalytic Activity. *RSC Adv.* **2017**, *7*, 10235–10241. [CrossRef]
20. Li, L.; Ai, L.; Zhang, C.; Jiang, J. Hierarchical {001}-Faceted BiOBr Microspheres as a Novel Biomimetic Catalyst: Dark Catalysis towards Colorimetric Biosensing and Pollutant Degradation. *Nanoscale* **2014**, *6*, 4627. [CrossRef]
21. Xing, H.; Ma, H.; Fu, Y.; Zhang, X.; Dong, X.; Zhang, X. Preparation of BiOBr by Solvothermal Routes with Different Solvents and Their Photocatalytic Activity. *J. Renew. Sustain. Energy* **2015**, *7*, 063120. [CrossRef]
22. Liu, Z.; Wu, B.; Xiang, D.; Zhu, Y. Effect of Solvents on Morphology and Photocatalytic Activity of BiOBr Synthesized by Solvothermal Method. *Mater. Res. Bull.* **2012**, *47*, 3753–3757. [CrossRef]
23. Li, R.; Ren, H.; Ma, W.; Hong, S.; Wu, L.; Huang, Y. Synthesis of BiOBr Microspheres with Ethanol as Self-Template and Solvent with Controllable Morphology and Photocatalytic Activity. *Catal. Commun.* **2018**, *106*, 1–5. [CrossRef]
24. Li, J.; Sun, S.; Qian, C.; He, L.; Chen, K.K.; Zhang, T.; Chen, Z.; Ye, M. The Role of Adsorption in Photocatalytic Degradation of Ibuprofen under Visible Light Irradiation by BiOBr Microspheres. *Chem. Eng. J.* **2016**, *297*, 139–147. [CrossRef]
25. Fang, Y.; Hua, T.; Feng, W.; Johnson, D.M.; Huang, Y. Mannitol Ligand-Assisted Assembly of BiOBr Photocatalyst in the Cationic Micelles of Cetylpyridinium Bromide. *Catal. Commun.* **2016**, *80*, 15–19. [CrossRef]

26. Hu, J.; Weng, S.; Zheng, Z.; Pei, Z.; Huang, M.; Liu, P. Solvents Mediated-Synthesis of BiOI Photocatalysts with Tunable Morphologies and Their Visible-Light Driven Photocatalytic Performances in Removing of Arsenic from Water. *J. Hazard. Mater.* **2014**, *264*, 293–302. [CrossRef] [PubMed]
27. Wang, X.; Li, F.; Li, D.; Liu, R.; Liu, S. Facile Synthesis of Flower-like BiOI Hierarchical Spheres at Room Temperature with High Visible-Light Photocatalytic Activity. *Mater. Sci. Eng. B* **2015**, *193*, 112–120. [CrossRef]
28. Gnayem, H.; Sasson, Y. Hierarchical Nanostructured 3D Flowerlike $BiOCl_x$ Br_{1-x} Semiconductors with Exceptional Visible Light Photocatalytic Activity. *ACS Catal.* **2013**, *3*, 186–191. [CrossRef]
29. Shi, X.; Chen, X.; Chen, X.; Zhou, S.; Lou, S.; Wang, Y.; Yuan, L. PVP Assisted Hydrothermal Synthesis of BiOBr Hierarchical Nanostructures and High Photocatalytic Capacity. *Chem. Eng. J.* **2013**, *222*, 120–127. [CrossRef]
30. Liu, J.; Hu, J.; Ruan, L.; Wu, Y. Facile and Environment Friendly Synthesis of Hierarchical BiOCl Flowery Microspheres with Remarkable Photocatalytic Properties. *Chin. Sci. Bull.* **2014**, *59*, 802–809. [CrossRef]
31. Zhao, Y.; Tan, X.; Yu, T.; Wang, S. SDS-Assisted Solvothermal Synthesis of BiOBr Microspheres with Highly Visible-Light Photocatalytic Activity. *Mater. Lett.* **2016**, *164*, 243–247. [CrossRef]
32. Wang, X.; Chen, H.; Li, H.; Mailhot, G.; Dong, W. Preparation and Formation Mechanism of BiOCl0.75I0.25 Nanospheres by Precipitation Method in Alcohol–Water Mixed Solvents. *J. Colloid Interface Sci.* **2016**, *478*, 1–10. [CrossRef]
33. Gao, X.; Zhang, X.; Wang, Y.; Peng, S.; Yue, B.; Fan, C. Rapid Synthesis of Hierarchical BiOCl Microspheres for Efficient Photocatalytic Degradation of Carbamazepine under Simulated Solar Irradiation. *Chem. Eng. J.* **2015**, *263*, 419–426. [CrossRef]
34. Yang, J.; Xie, T.; Zhu, Q.; Wang, J.; Xu, L.; Liu, C. Boosting the Photocatalytic Activity of BiOX under Solar Light via Selective Crystal Facet Growth. *J. Mater. Chem. C* **2020**, *8*, 2579–2588. [CrossRef]
35. Zhang, H.; Yang, Y.; Zhou, Z.; Zhao, Y.; Liu, L. Enhanced Photocatalytic Properties in BiOBr Nanosheets with Dominantly Exposed (102) Facets. *J. Phys. Chem. C* **2014**, *118*, 14662–14669. [CrossRef]
36. Dai, B.; Zhang, A.; Liu, Z.; Wang, T.; Li, C.; Zhang, C.; Li, H.; Liu, Z.; Zhang, X. Facile Synthesis of Metallic Bi Deposited BiOI Composites with the Aid of EDTA-2Na for Highly Efficient Hg0 Removal. *Catal. Commun.* **2019**, *121*, 53–56. [CrossRef]
37. Chang, C.; Zhu, L.; Fu, Y.; Chu, X. Highly Active Bi/BiOI Composite Synthesized by One-Step Reaction and Its Capacity to Degrade Bisphenol A under Simulated Solar Light Irradiation. *Chem. Eng. J.* **2013**, *233*, 305–314. [CrossRef]
38. Montoya-Zamora, J.M.; Martínez-de la Cruz, A.; López Cuéllar, E. Enhanced Photocatalytic Activity of BiOI Synthesized in Presence of EDTA. *J. Taiwan Inst. Chem. Eng.* **2017**, *75*, 307–316. [CrossRef]
39. Bárdos, E.; Márta, V.; Baia, L.; Todea, M.; Kovács, G.; Baán, K.; Garg, S.; Pap, Z.; Hernadi, K. Hydrothermal Crystallization of Bismuth Oxybromide (BiOBr) in the Presence of Different Shape Controlling Agents. *Appl. Surf. Sci.* **2020**, *518*, 146184. [CrossRef]
40. Hu, T.; Li, H.; Zhang, R.; Du, N.; Hou, W. Thickness-Determined Photocatalytic Performance of Bismuth Tungstate Nanosheets. *RSC Adv.* **2016**, *6*, 31744–31750. [CrossRef]
41. Zhang, G.; Cai, L.; Zhang, Y.; Wei, Y. Bi^{5+}, $Bi^{(3-x)+}$, and Oxygen Vacancy Induced $BiOCl_x$ I_{1-x} Solid Solution toward Promoting Visible-Light Driven Photocatalytic Activity. *Chem. Eur. J.* **2018**, *24*, 7434–7444. [CrossRef]
42. Heidari, S.Z.; Haghighi, M.; Shabani, M. Sunlight-activated BiOCl/BiOBr–$Bi_{24}O_{31}Br_{10}$ photocatalyst for the removal of pharmaceutical compounds. *J. Clean. Prod.* **2020**, *259*, 120679. [CrossRef]
43. Lin, Z.; Zhe, F.; Wang, Y.; Zhang, Q.; Zhao, X.; Hu, X.; Wu, Y.; He, Y. Preparation of interstitial carbon doped BiOI for enhanced performance in photocatalytic nitrogen fixation and methyl orange degradation. *J. Colloid Interface Sci.* **2019**, *539*, 563–574. [CrossRef]
44. Zhang, H.; Liu, L.; Zhou, Z. First-Principles Studies on Facet-Dependent Photocatalytic Properties of Bismuth Oxyhalides (BiOXs). *RSC Adv.* **2012**, *2*, 9224. [CrossRef]
45. Weng, S.; Fang, Z.; Wang, Z.; Zheng, Z.; Feng, W.; Liu, P. Construction of Teethlike Homojunction BiOCl (001) Nanosheets by Selective Etching and Its High Photocatalytic Activity. *ACS Appl. Mater. Interfaces* **2014**, *6*, 18423–18428. [CrossRef] [PubMed]
46. Gao, M.; Zhang, D.; Pu, X.; Li, H.; Li, J.; Shao, X.; Ding, K. BiOBr Photocatalysts with Tunable Exposing Proportion of {001} Facets: Combustion Synthesis, Characterization, and High Visible-Light Photocatalytic Properties. *Mater. Lett.* **2015**, *140*, 31–34. [CrossRef]
47. Xu, J.; Meng, W.; Zhang, Y.; Li, L.; Guo, C. Photocatalytic Degradation of Tetrabromobisphenol A by Mesoporous BiOBr: Efficacy, Products and Pathway. *Appl. Catal. B Environ.* **2011**, *107*, 355–362. [CrossRef]
48. Zhang, L.; Cao, X.-F.; Chen, X.-T.; Xue, Z.-L. BiOBr Hierarchical Microspheres: Microwave-Assisted Solvothermal Synthesis, Strong Adsorption and Excellent Photocatalytic Properties. *J. Colloid Interface Sci.* **2011**, *354*, 630–636. [CrossRef]
49. Arumugam, M.; Choi, M.Y. Recent Progress on Bismuth Oxyiodide (BiOI) Photocatalyst for Environmental Remediation. *J. Ind. Eng. Chem.* **2020**, *81*, 237–268. [CrossRef]
50. Xiao, X.; Xing, C.; He, G.; Zuo, X.; Nan, J.; Wang, L. Solvothermal Synthesis of Novel Hierarchical $Bi_4O_5I_2$ Nanoflakes with Highly Visible Light Photocatalytic Performance for the Degradation of 4-Tert-Butylphenol. *Appl. Catal. B Environ.* **2014**, *148*, 154–163. [CrossRef]
51. Fan, Z.; Zhao, Y.; Zhai, W.; Qiu, L.; Li, H.; Hoffmann, M.R. Facet-Dependent Performance of BiOBr for Photocatalytic Reduction of Cr(VI). *RSC Adv.* **2016**, *6*, 2028–2031. [CrossRef]

52. Hussain, M.B.; Khan, M.S.; Loussala, H.M.; Bashir, M.S. The Synthesis of a $BiOCl_x Br_{1-x}$ Nanostructure Photocatalyst with High Surface Area for the Enhanced Visible-Light Photocatalytic Reduction of Cr(VI). *RSC Adv.* **2020**, *10*, 4763–4771. [CrossRef]
53. Li, H.; Deng, F.; Zheng, Y.; Hua, L.; Qu, C.; Luo, X. Visible-Light-Driven Z-Scheme RGO/Bi_2S_3 –BiOBr Heterojunctions with Tunable Exposed BiOBr (102) Facets for Efficient Synchronous Photocatalytic Degradation of 2-Nitrophenol and Cr(VI) Reduction. *Environ. Sci. Nano* **2019**, *6*, 3670–3683. [CrossRef]